

# Supporting Information

## Fluorophosphates as Efficient Bifunctional Electrocatalysts for Metal-air Batteries

Lalit Sharma,<sup>†</sup> Ritambhara Gond,<sup>†</sup> Baskar Senthilkumar,<sup>†</sup> Ahin Roy,<sup>‡</sup> and Prabeer Barpanda<sup>†\*</sup>

<sup>†</sup>Faraday Materials Laboratory, Materials Research Center,  
Indian Institute of Science, C. V. Raman Avenue, Bangalore, 560012, India.

<sup>‡</sup>Materials Research Center,  
Indian Institute of Science, C. V. Raman Avenue, Bangalore, 560012, India.

\*author for correspondence

E-mail: [prabeer@iisc.ac.in](mailto:prabeer@iisc.ac.in)

Phone: +91-80 2293 2783; Fax: +91-80 2360 7316

---

### 1. Experimental Section:

#### 1.1. Synthesis of carbon-coated porous Na<sub>2</sub>CoPO<sub>4</sub>F

Na<sub>2</sub>CoPO<sub>4</sub>F fluorophosphates was prepared by combustion synthesis. Stoichiometric amounts of Co(NO<sub>3</sub>)<sub>2</sub>·6H<sub>2</sub>O (SDFCL, 99%), NaH<sub>2</sub>PO<sub>4</sub> (Fluka, 99%), NaF (Merck, 99%) and C<sub>6</sub>H<sub>8</sub>O<sub>7</sub> (SDFCL, 99%) were dissolved in water. Citric acid acts as a fuel as well as a source of carbon. To achieve the optimum combustion, the amount of fuel was calculated by taking into account the combustion index of each element as described in earlier reports.<sup>1, 2</sup> The solution was heated at 140 °C with continuous magnetic stirring to remove excess water and to trigger an exothermic combustion reaction yielding pink colored combustion ash. It was ground, pelletized and was annealed inside a tubular furnace at 600 °C for 6 hours under steady Ar flow to obtain the final Na<sub>2</sub>CoPO<sub>4</sub>F product.

## 1.2. Physical characterization of Na<sub>2</sub>CoPO<sub>4</sub>F

Powder diffraction patterns were acquired with a PANalytical X'Pert Pro diffractometer using a Cu-K $\alpha$  source ( $\lambda_1 = 1.5408 \text{ \AA}$ ,  $\lambda_2 = 1.5443 \text{ \AA}$ ) operating at 40 kV/30 mA. The patterns were collected in  $2\theta$  range of 10-100° with a step size of 0.026° s<sup>-1</sup>. Rietveld refinement was carried out using GSAS program with EXPGUI front end.<sup>3-5</sup> Particle morphology was observed with a field emission gun scanning electron microscope (FEI Inspect F50) (operating at 5-20 kV/ 3-4  $\mu$ A) and a Tecnai T20 super twin transmission electron microscope equipped with a W-filament (operating at 200 kV). To prepare the TEM sample, 1 mg powder was well-dispersed in 5 mL acetone through ultrasonication, which was drop cast on a carbon coated Cu-grid. Porosity and active surface area were measured by the Brunauer-Emmett-Teller (BET) method resulting from the measurement of N<sub>2</sub> gas (de)adsorption isotherms with a Quantachrome automated gas sorption analyzer. Raman spectra were acquired with a LabRam HR Evolution spectrometer (HORIBA, Japan) using a 514.5 nm (green) laser source with a spectral resolution of 1 cm<sup>-1</sup> and a spatial resolution of 2.5 nm. Infrared spectra of powder samples (diluted in KBr pellets) were obtained with a Perkin Elmer 1000 FTIR spectrometer in the wavenumber range of 400-4000 cm<sup>-1</sup> (cycle number = 4).

## 1.3. Electrochemical characterization of Na<sub>2</sub>CoPO<sub>4</sub>F

For electrochemical testing, 2032 coin type half cells were assembled inside an Ar-filled glove box. A slurry with active material, carbon black and polyvinylidene fluoride (PVDF) binder, in 80:10:10 w/w ratio, was prepared in N-methyl-pyrrolidone (NMP) and casted on aluminium foil. It was dried overnight at 80 °C. Sodium metal was used as anode with 1 M NaPF<sub>6</sub> dissolved in ethylene carbonate and di-ethyl carbonate (1:1 v/v ratio) as electrolyte. Glass fiber sheet was used as a separator. The cells were cycled in the voltage range of 2.0 – 5.0 V (at 25 °C) at a rate of C/20 using Bio-Logic BCS 805/810 automatic battery tester.

#### 1.4. Na-ion diffusivity in Na<sub>2</sub>CoPO<sub>4</sub>F

Bond valence site energy (BVSE) calculations were performed to analyze Na-ion diffusion pathway in Na<sub>2</sub>CoPO<sub>4</sub>F. Methodology of BVSE based on molecular dynamics simulation has been discussed in detail elsewhere.<sup>6-8</sup> Simplest and reliable tool to model Na ion pathways and migration barriers (via BVSE) is to consider these ions to have a region of low bond valence site energy  $E_{BVSE}(\text{Na}^+)$ .<sup>8,9</sup>

BV ion transport calculation involves empirical relationships between the bond length,  $R$  and a so called bond valence,  $s_{\text{Na-X}}$ , which can be expressed as  $s_{\text{Na-X}} = \exp[(R_{0,\text{Na-X}} - R_{\text{Na-X}})/b_{\text{Na-X}}]$ . The bond valence (BV) sum mismatch  $|\Delta V|$  are basically expressed in arbitrary “valence units”, as elaborated in the previous reports.<sup>10-12</sup> The  $s_{\text{Na-X}}$  and  $|\Delta V|$  are linked to an absolute energy scale by expressing the squared bond valence as a Morse-type interaction energy between Na<sup>+</sup> cation and O<sup>2-</sup> as well as F<sup>-</sup> anion represented as X.

$$E_{BVSE}(\text{Na-X}) = \sum_x D \left[ \sum_{i=1}^N \left( \left( \frac{s_{\text{Na-X}}}{s_{\text{min,Na-X}}} \right)^2 - 2 \frac{s_{\text{Na-X}}}{s_{\text{min,Na-X}}} \right) \right] + E_{repulsion} \quad (1)$$

Here,  $s_{\text{min,Na-X}}$  corresponds to the expected BV of a Na-X bond at the equilibrium distance  $R_{\text{min,Na-X}}$ .  $D$  is the bond breaking energy that can be derived as a function of  $R_{\text{min}}$ , the oxidation state  $V_{\text{Na}} = 1$ ,  $V_{\text{X}}$  of Na and X, the bond softness parameter  $b$  and the period number of Na and X as

$$D_0 = \varepsilon_0 \frac{b^2}{2R_{\text{min}}} \frac{V_{\text{Na}} |V_{\text{X}}|}{\sqrt{n_{\text{Na}} n_{\text{X}}}} \quad (2)$$

All required bond valence parameters were obtained from the *softBV* database.<sup>11</sup> Regions of low bond valence site energy  $E_{BVSE}(\text{Na})$ , discussed before in grids spanning the structure model with a resolution of 0.1 Å<sup>3</sup>, were investigated for Na<sup>+</sup> migration pathways in Na<sub>2</sub>CoPO<sub>4</sub>F. Required initial structure model for BVSE calculations was obtained using Rietveld refined X-ray Powder diffraction of Na<sub>2</sub>CoPO<sub>4</sub>F sample.

### 1.5. Electrode preparation for electrocatalytic characterization

For electrocatalytic study, slurry was prepared in 1000  $\mu\text{L}$  solution (250  $\mu\text{L}$  iso-propyl alcohol and 750  $\mu\text{L}$  distilled water) with 10 mg active material, 5 mg Super P and 5  $\mu\text{L}$  Nafion as binder. For intimate mixing, the slurry was sonicated for 30 minutes after adding Nafion. The slurry was cast on glassy carbon rotating ring disc electrode (RRDE). The active material loading was optimized by testing different slurry coatings at room temperature on CH instruments (CHI700E) bipotentiostat using 0.1 M NaOH as electrolyte.

### 1.6. Preparation and configuration of aqueous Na-air battery

For sodium air-cathode preparation, an intimate slurry of sodium cobalt fluorophosphate  $\text{Na}_2\text{CoPO}_4\text{F}$ , conductive carbon black Super-P (Sigma Aldrich) and polyvinylidene fluoride (PVDF, Sigma Aldrich) binder (w/w ratio 80:10:10) in N-methyl-pyrrolidone (NMP) was prepared and was coated on carbon paper. A NASICON-type  $\text{Na}_3\text{Zr}_2\text{Si}_2\text{P}_3\text{O}_{12}$  ceramic pellet was used as the solid electrolyte.  $\text{Na}_3\text{Zr}_2\text{Si}_2\text{P}_3\text{O}_{12}$  was prepared by a solid-state reaction involving mixing of  $\text{Na}_3\text{PO}_4 \cdot 12\text{H}_2\text{O}$ ,  $\text{SiO}_2$  and  $\text{ZrO}_2$  precursors followed by calcination at 400 and 1100  $^\circ\text{C}$ .<sup>13</sup> The resulting product powder was ground, pelletized and was subjected to a final sintering step at 1230  $^\circ\text{C}$ . Na metal foil was used as anode attached to 9  $\text{mm}^2$  Ni mesh acting as current collector. The anode part (pouch cell) was assembled inside an Ar-filled MBraun GmbH glove box maintaining  $\text{O}_2/\text{H}_2\text{O}$  level below 1 ppm. The final cell configuration can be written as (-) Ni mesh | metallic Na | organic electrolyte | NASICON | 0.1 M NaOH |  $\text{Na}_2\text{CoPO}_4\text{F}$  | Ti mesh (+).

## References

- (1) Barpanda, P.; Ye, T.; Chung, S. C.; Yamada, Y.; Nishimura, S.; Yamada, A. Eco-efficient Splash Combustion Synthesis of Nanoscale Pyrophosphate ( $\text{Li}_2\text{FeP}_2\text{O}_7$ ) Positive-electrode using Fe(III) Precursors. *J. Mater. Chem.*, **2012**, *22*, 13455-13459.
- (2) Barpanda, P.; Yamashita, Y.; Yamada, Y.; Yamada, A. High-throughput Solution Combustion Synthesis of High-capacity  $\text{LiFeBO}_3$  Cathode. *J. Electrochem. Soc.* **2013**, *160*, A3095-A3099.
- (3) Rietveld, H. M. A Profile Refinement Method for Nuclear and Magnetic Structures. *J. Appl. Crystallogr.* **1969**, *2*, 65-71.
- (4) Larson, A. C.; Dreele, R. B. V. *General Structure Analysis System (GSAS)*; Los Alamos National Laboratory Report, LAUR 86-748; Los Alamos National Laboratory: Los Alamos, NM, **1994**.
- (5) Toby, B. H. *EXPGUI*, A Graphical User Interface for *GSAS*. *J. Appl. Crystallogr.* **2001**, *34*, 210-213.
- (6) Adams, S.; Rao, R. P. Understanding Ionic Conduction and Energy Storage Materials with Bond-valence-based Methods. *Structure and Bonding* **2014**, *158*, 129-159.
- (7) Adams, S. Lithium Ion Pathways in  $\text{LiFePO}_4$  and Related Olivines. *J. Solid State Electrochem.* **2010**, *14*, 1787-1792.
- (8) Adams, S.; Rao, R. P. Structural Requirements for Fast Lithium Ion Migration in  $\text{Li}_{10}\text{GeP}_2\text{S}_{12}$ . *J. Mater. Chem.* **2012**, *22*, 7687-7691.
- (9) Adams, S.; Rao, R. P. Ion Transport and Phase Transition in  $\text{Li}_{7-x}\text{La}_3(\text{Zr}_{2-x}\text{M}_x)\text{O}_{12}$  ( $\text{M}=\text{Ta}^{5+}, \text{Nb}^{5+}$ ,  $x=0, 0.25$ ). *J. Mater. Chem.* **2012**, *22*, 1426-1434.
- (10) Adams, S.; Rao, R. P. Transport Pathways for Mobile Ions in Disordered Solids from the Analysis of Energy-scaled Bond-valence Mismatch Landscapes. *Phys. Chem. Chem. Phys.* **2009**, *11*, 3210-3216.

(11) Adams, S. Practical Considerations in Determining Bond Valence Parameters, in *Bond Valences*, ed. I. D. Brown and K. R. Poeppelmeier, Springer, Berlin Heidelberg, *Structure and Bonding*, 2014, **158**, 91–128.

(12) Adams, S.; Rao, R. P. Simulated Defect and Interface Engineering for High Power Li Electrode Materials. *Solid State Ionics* **2011**, *184*, 57-61.

(13) Kim, J. K.; Lee, E.; Kim, H.; Johnson, C.; Cho, J.; Kim, Y. Rechargeable Seawater Battery and its Electrochemical Mechanism. *ChemElectroChem* **2015**, *2*, 328-332.

**Table S1.** Crystallographic data, lattice parameter and atomic coordinates of Na<sub>2</sub>CoPO<sub>4</sub>F compound derived from Rietveld refinement.

<b>Na<sub>2</sub>CoPO<sub>4</sub>F</b>	
Formula Weight	Na <sub>2</sub> CoPO <sub>4</sub> F [218.88 g mol <sup>-1</sup> ]
Temperature (K)	298
Crystal System	Orthorhombic
Space group	<i>Pbcn</i>
Unit cell parameter (Å)	$a = 5.246(4), b = 13.785(3), c = 11.677(5)$ $\alpha = \beta = \gamma = 90^\circ, Z = 8$
Unit cell volume (Å <sup>3</sup> )	844.5(7)
Theoretical Density (g cm <sup>-3</sup> )	3.44
Fitness parameters (R values)	$R_p = 3.24, R_{wp} = 6.53, \chi^2 = 3.683$

<b>Atoms</b>	<b>x</b>	<b>y</b>	<b>z</b>	<b>Occ.</b>	<b>U<sub>iso</sub>(Å<sup>2</sup>)</b>	<b>Wykoff position</b>
Co1	0.2411(0)	0.4818(6)	0.6725(7)	1	0.012	8d
P1	-0.2867(8)	0.6173(9)	0.5922(3)	1	0.093	8d
Na1	0.2547(1)	0.6359(9)	0.4183(9)	1	0.019	8d
Na2	0.2489(8)	0.2489(5)	0.6688(3)	1	0.048	8d
F1	0.5000(0)	0.3969(8)	0.7500(0)	1	0.101	4c
F2	0	0.3777(8)	0.7500(0)	1	0.203	4c
O1	-0.2076(4)	0.5404(9)	0.6757(7)	1	0.074	8d
O2	-0.2368(4)	0.7218(7)	0.6232(4)	1	0.016	8d
O3	0.4139(6)	0.6125(8)	0.5969(5)	1	0.036	8d
O4	0.2328(7)	0.3874(1)	0.5351(1)	1	0.043	8d

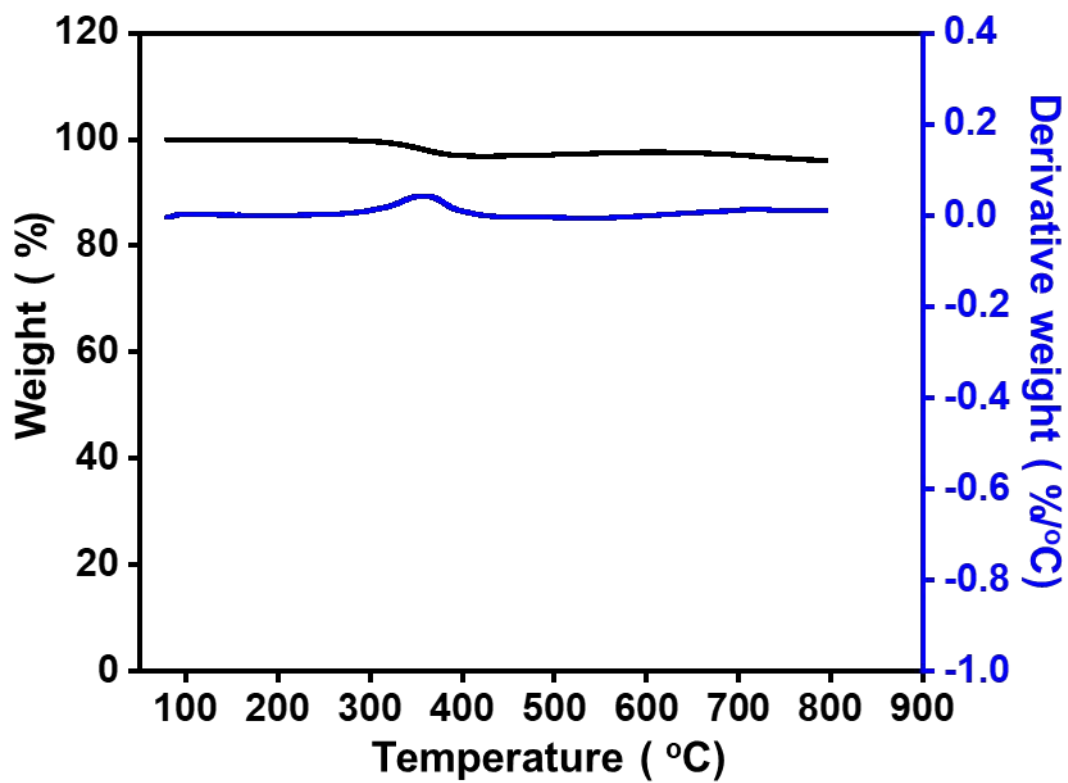


**Figure S1:** TG-DTA curve of Na<sub>2</sub>CoPO<sub>4</sub>F ash in argon atmosphere showing the thermal stability of the material with only slight decomposition at approximately 500 °C.

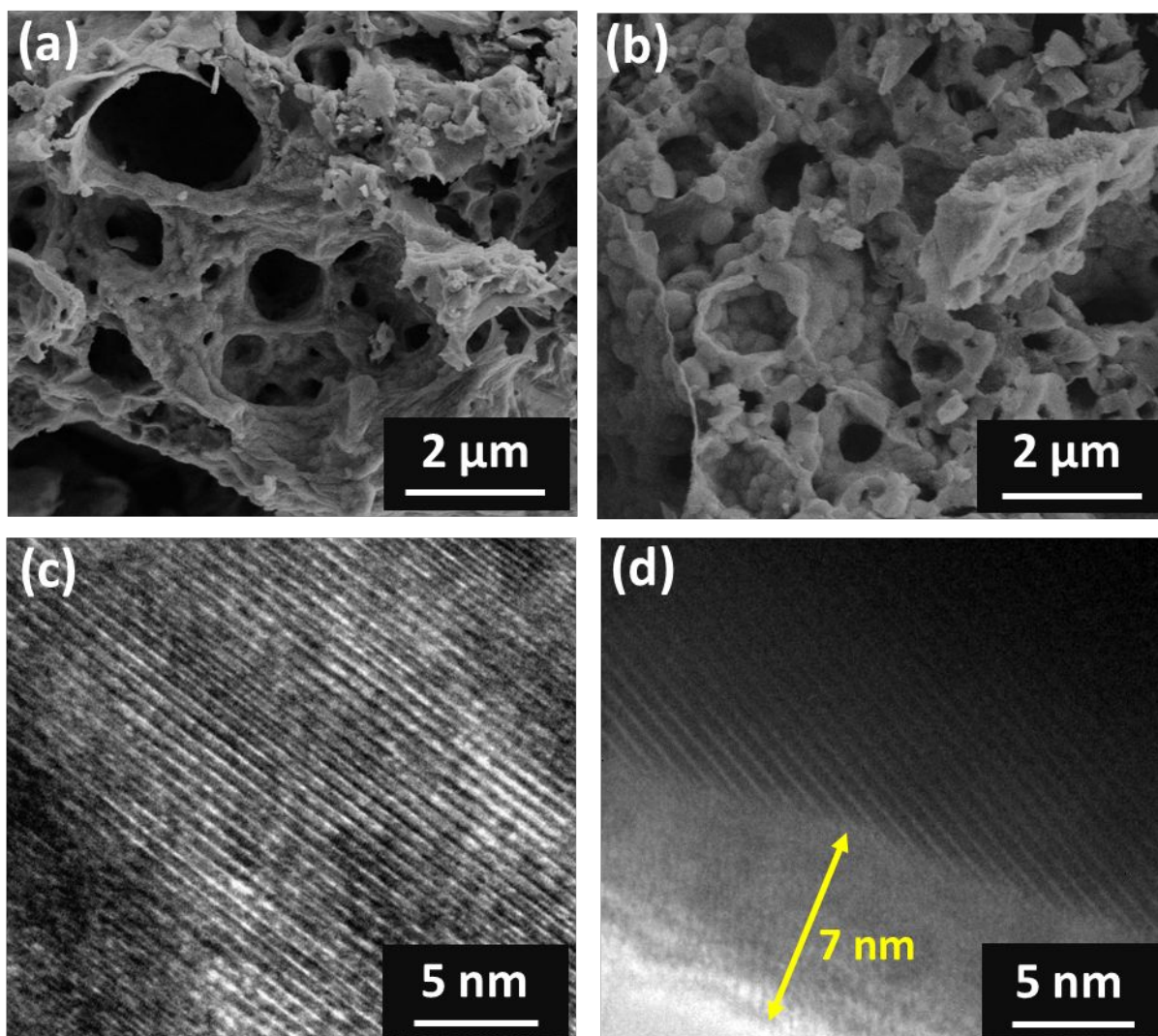


**Figure S2:** (a-b) Scanning electron micrographs of  $\text{Na}_2\text{CoPO}_4\text{F}$  showing the presence of huge amount of porosity, (c) High resolution transmission electron micrograph indicating the crystallinity of the material, (d) TEM micrograph showing the presence of carbon-coating on the surface of grains.

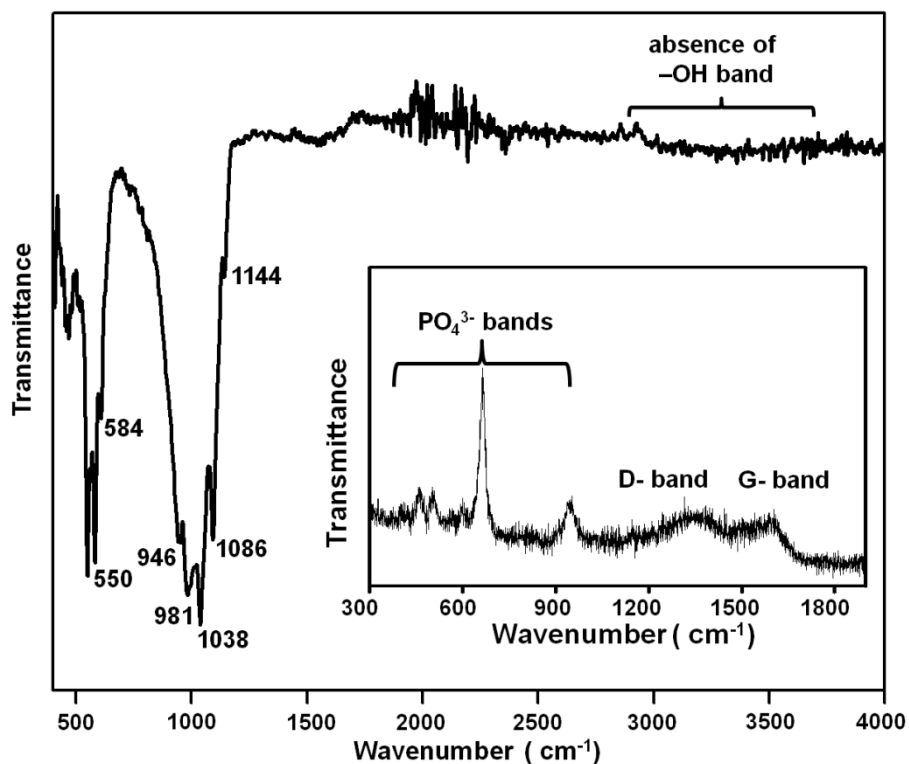


**Figure S3:** FTIR -spectra of as-synthesized Na<sub>2</sub>CoPO<sub>4</sub>F, peaks around 600 cm<sup>-1</sup> and 1100 cm<sup>-1</sup> indicate presence of phosphate functional group while no broad peak between 3600 to 2600 cm<sup>-1</sup> shows absence of any adsorbed water. Inset: Presence of carbon coating was confirmed by the presence of D-band and G-band in Raman Spectra.

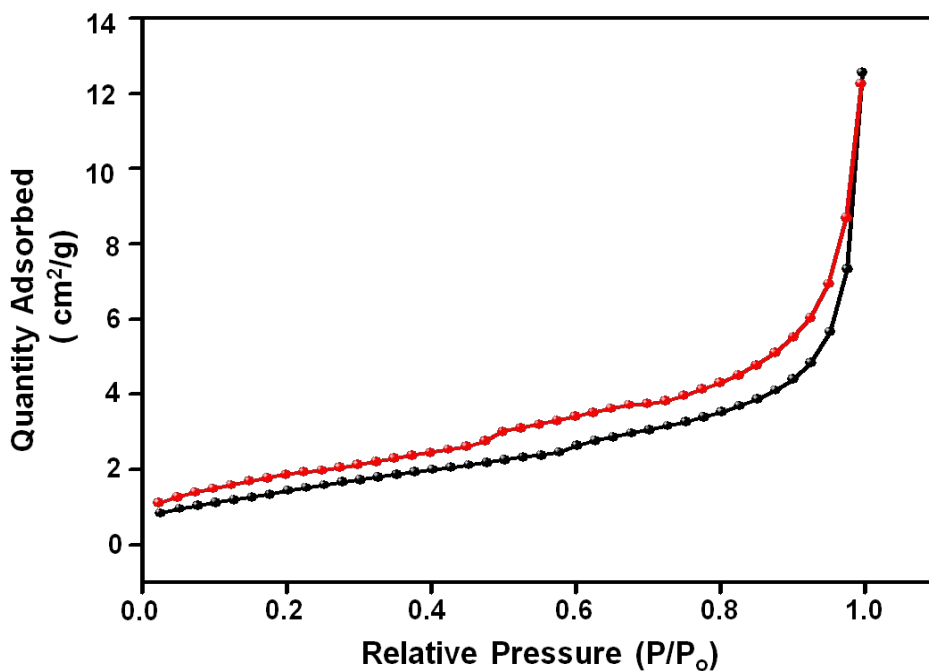


**Figure S4:** BET (de)adsorption isotherm of  $\text{Na}_2\text{CoPO}_4\text{F}$  showing macro-porosity and an active surface area of  $8 \text{ m}^2 \text{ g}^{-1}$ .

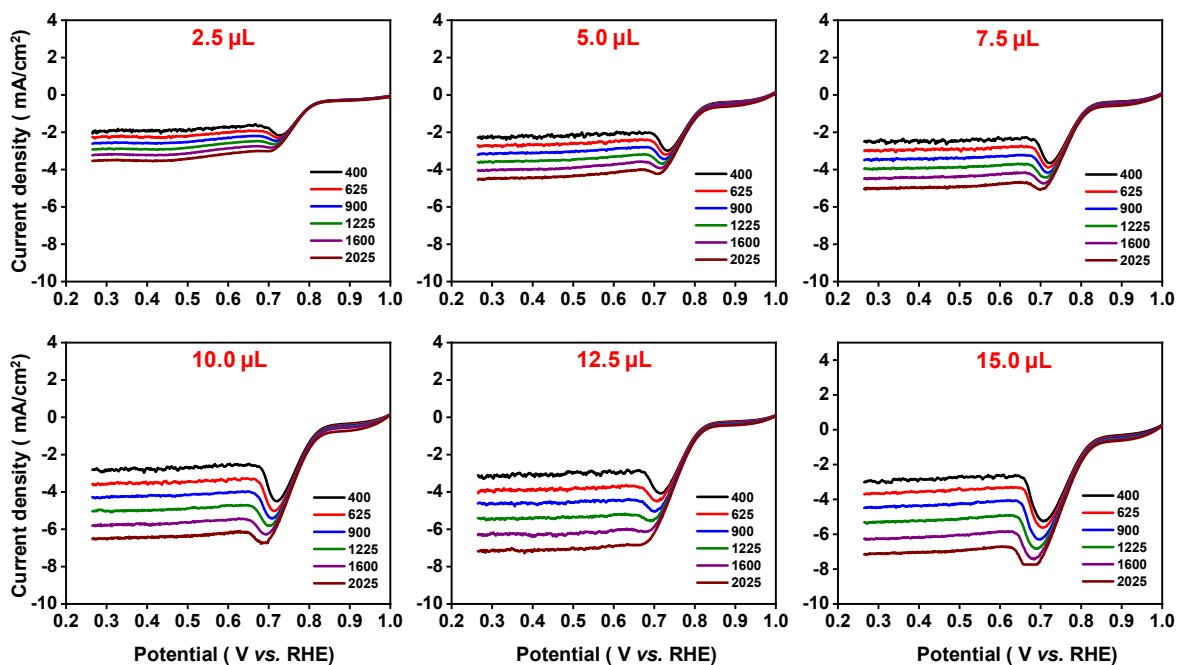


**Figure S5:** LSV plots of different active material loading recorded at different rpm (400-2200 rpm) to optimize the loading.

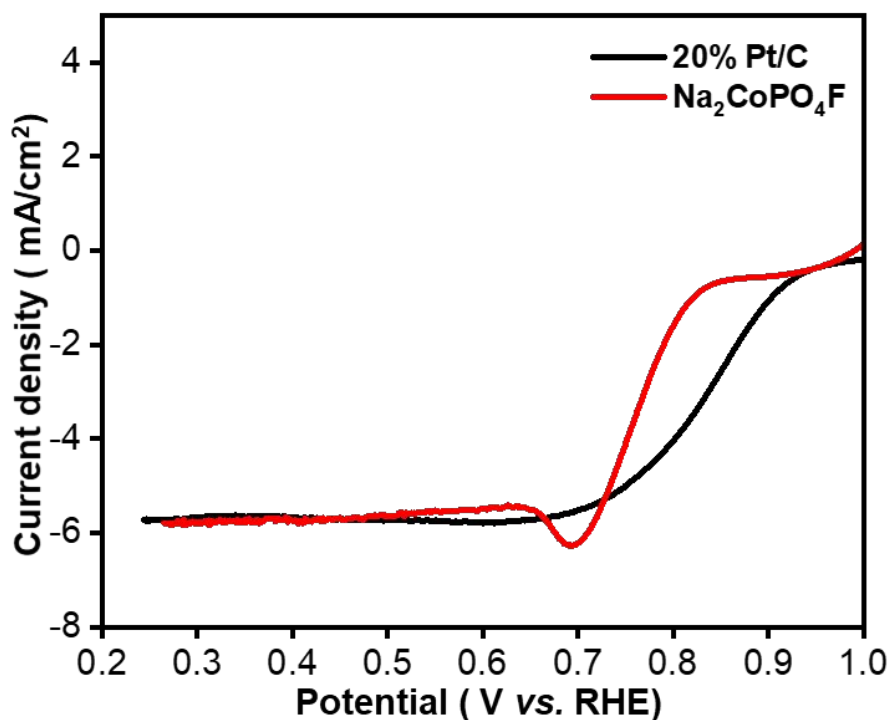


**Figure S6:** Linear sweep voltammogram (LSV) of benchmarked 20% Pt/C and  $\text{Na}_2\text{CoPO}_4\text{F}$  during oxygen reduction reaction recorded at 1600 rpm showing similar limiting current densities for both material.

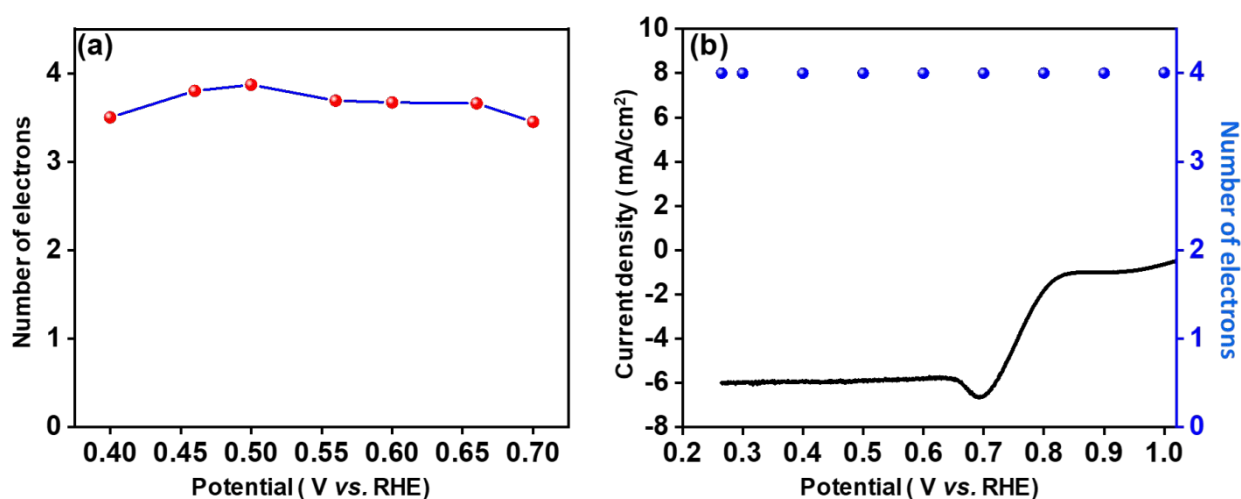


**Figure S7:** Calculation of number of electrons involved during ORR mechanism using (a) Koutecky-Levich (K-L) plot at different potential, (b) ring current.

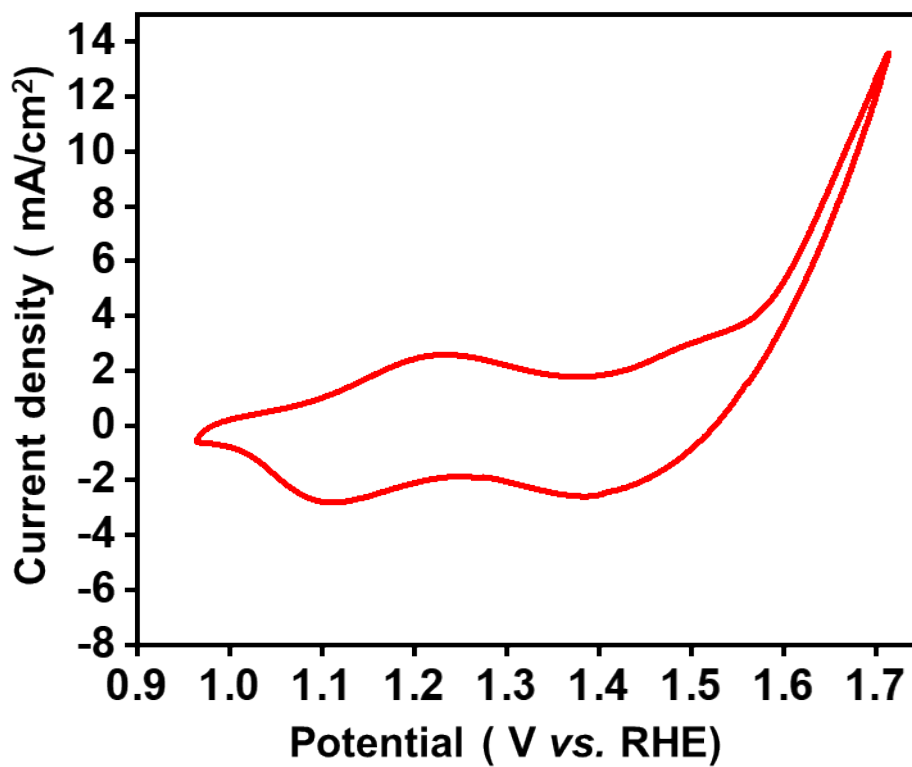


**Figure S8:** Cyclic voltammetry carried out at 1600 rpm during OER process having two well defined redox peaks corresponding to  $\text{Co}^{2+}/\text{Co}^{3+}$  and  $\text{Co}^{3+}/\text{Co}^{4+}$  and an onset potential of 1.591 V vs. RHE.

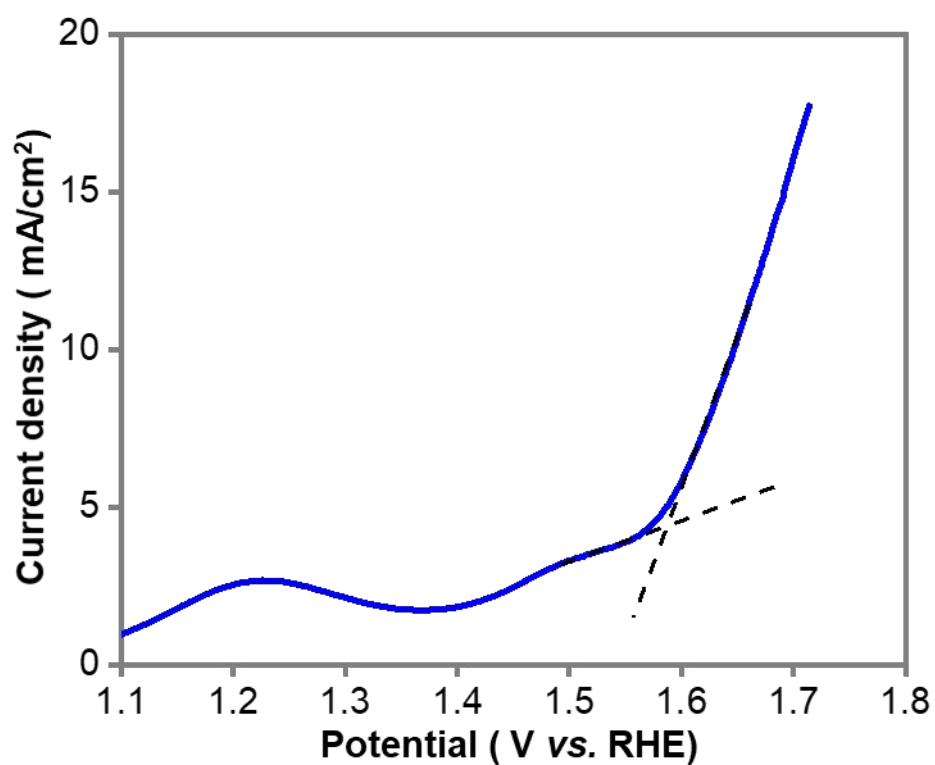


**Figure S9:** Linear sweep voltammogram (LSV) of  $\text{Na}_2\text{CoPO}_4\text{F}$  during oxygen evolution reaction recorded at 1600 rpm between 1.1 to 1.7 V vs. RHE showing the onset potential and current density.

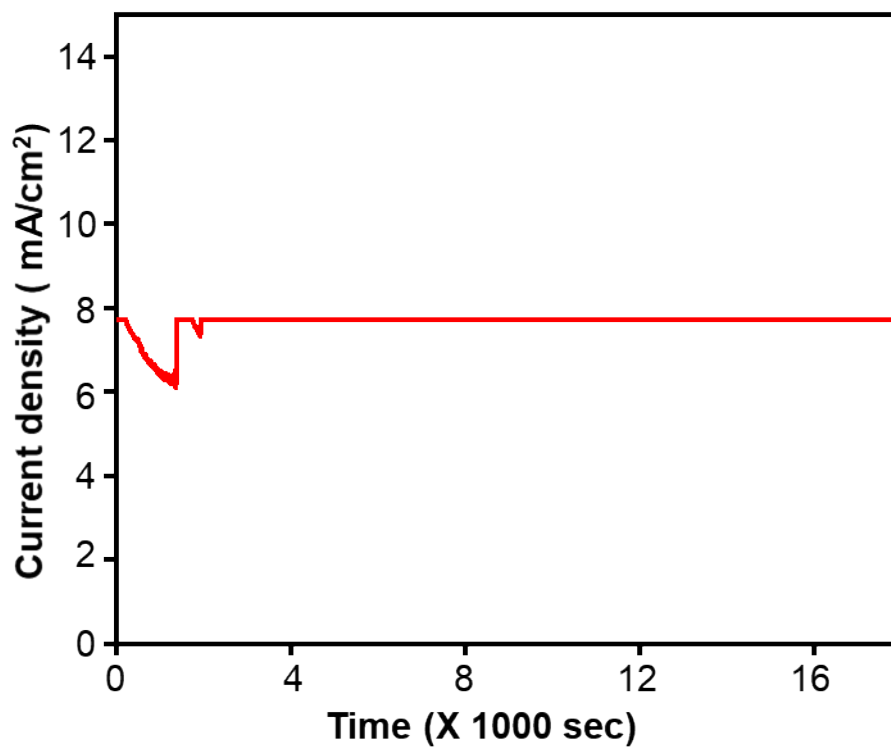


**Figure S10:** OER stability of  $\text{Na}_2\text{CoPO}_4\text{F}$  carried out for 5 hours using chronoamperometric technique at 1600 rpm. Initial current loss corresponds to the huge  $\text{O}_2$  bubble formation at the surface and structural reorientation in the material. However, no current loss was observed for 5 hours showing its good OER stability.

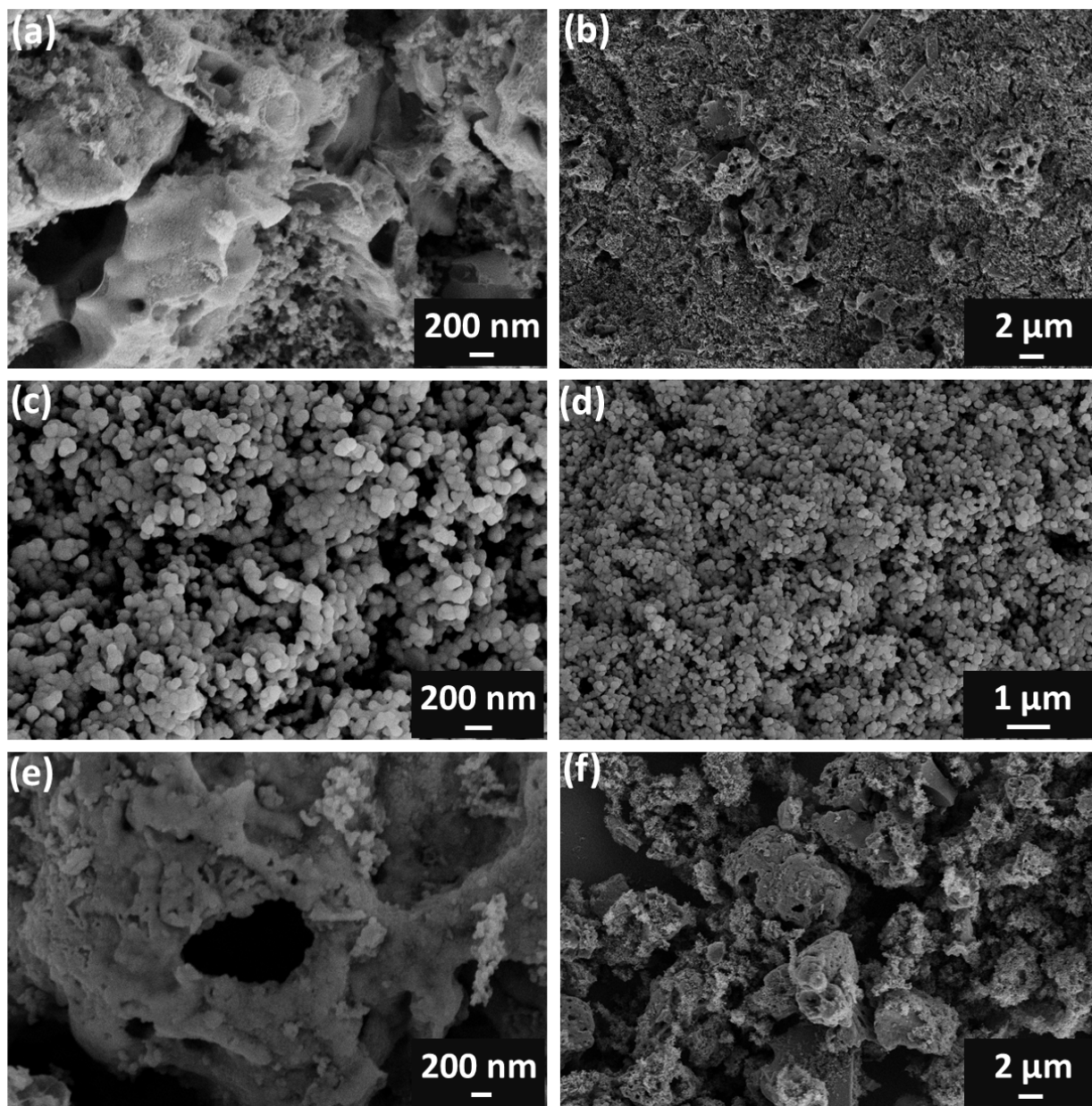


**Figure S11:** SEM images of (a, b) slurry of  $\text{Na}_2\text{CoPO}_4\text{F}$  coated on RRDE; (c, d) material recovered after undergoing 10 cycles of ORR; (e, f) material recovered after 10 cycles of OER. The disintegration of bigger particles into smaller ones is clearly visible.